Computational and Structural Biotechnology Journal 20 (2022) 287–295

ELSEVIER

COMPUTATIONAL ANDSTRUCTURAL BIOTECHNOLOGY JOURNAL

journal homepage: www.elsevier.com/locate/csbj

Flow cytometry-based study of model marine microalgal consortia revealed an ecological advantage of siderophore utilization by the dinoflagellate *Amphidinium carterae*

Ronald Malych [a], Pavel Stopka [b], Jan Mach [a], Eva Kotabová [c], Ondřej Prášil [c], Robert Sutak [a,*]

[a] Department of Parasitology, Faculty of Science, Charles University, BIOCEV, Vestec, Czech
[b] Department of Zoology, Faculty of Science, Charles University, BIOCEV, Vestec, Czech
[c] Institute of Microbiology, Academy of Sciences, Centrum Algatech, Trebon, Czech

ARTICLE INFO

Article history:
Received 5 October 2021
Received in revised form 14 December 2021
Accepted 15 December 2021
Available online 20 December 2021

Keywords:
Amphidinium carterae
Flow cytometry
Iron
Marine microalgae
Proteomics
Siderophores

ABSTRACT

Investigations of phytoplankton responses to iron stress in seawater are complicated by the fact that iron concentrations do not necessarily reflect bioavailability. Most studies to date have been based on single species or field samples and are problematic to interpret. Here, we report results from an experimental cocultivation model system that enabled us to evaluate interspecific competition as a function of iron content and form, and to study the effect of nutritional conditions on the proteomic profiles of individual species. Our study revealed that the dinoflagellate *Amphidinium carterae* was able to utilize iron from a hydroxamate siderophore, a strategy that could provide an ecological advantage in environments where siderophores present an important source of iron. Additionally, proteomic analysis allowed us to identify a potential candidate protein involved in iron acquisition from hydroxamate siderophores, a strategy that is largely unknown in eukaryotic phytoplankton.

1. Introduction

The importance of iron for marine phytoplankton, a key nutrient controlling phytoplankton production in high nutrient/low chlorophyll ocean regions, has been known for three decades [1]. Consequently, phytoplankton employ a great diversity of strategies to overcome iron limitation, including reducing cell size and iron requirements [2], efficiently acquiring iron with iron uptake rates reaching the universal upper limit [3], utilizing xenosiderophores [4], and possessing iron storage mechanisms [5]. Considering the variability in chemical and biogeochemical aspects of iron, such as its concentration, form, distribution or seasonal variations in availability, it is extremely difficult to predict how phytoplankton communities will respond to changing iron conditions. Nevertheless, it is extremely important to understand the consequences of iron stress on phytoplankton considering the alterations in iron bioavailability and distribution that we expect due to global climate changes [6].

Cocultivation experiments represent powerful tools to study interspecific interactions, particularly for characterization of symbiosis and parasitism (e.g., [7,8]). The potential of cocultivation is now enhanced by a growing number of available microbial genomes and/or transcriptomes, as well as by the technical improvement and increased accessibility of omics techniques, particularly proteomics. In marine phytoplankton research, studies are mostly based on lab-scale experiments focused on single species or on investigations of complex field samples that are difficult to interpret. Nevertheless, lab-scale coculture studies of marine phytoplankton have revealed important findings, such as

Abbreviations: AtpE, ATP synthase; AUC, area under curve; BCS, bathocuproinedisulfonic acid disodium salt; CREG1, cellular repressor of E1A stimulated genes 1; DFOB, desferrioxamine B; EDTA, ethylenediaminetetraacetic acid; ENT, enterobactin; FACS, fluorescence-activated cell sorting; FBAI, fructose-bisphosphate aldolase I; FBAII, fructose-bisphosphate aldolase II; FBP1, putative ferrichrome-binding protein; FOB, ferrioxamine B; ISIP, iron starvation induced protein; LHCX, light-harvesting complex subunits; LL, long-term iron limitation; LR, iron enrichment; NBD, nitrobenz-2-oxa-1,3-diazole; NPQ, nonphotochemical quenching; PAGE, polyacrylamide gel electrophoresis; PetA, cytochrome b6/f; PSI, photosystem I; PSII, photosystem II; PsaC, photosystem I iron-sulfur center; PsaD, photosystem I reaction center subunit II; PsaE, photosystem I reaction center subunit IV; PsaL, photosystem I reaction center subunit XI; PsbC, photosystem II CP43 reaction center protein; PsbV, cytochrome *c*-550; RR, long-term iron sufficiency; (s)PLS-DA, (sparse) partial least squares discriminant analysis; SOD1, superoxide dismutase [Cu-Zn].

* Corresponding author.
E-mail address: sutak@natur.cuni.cz (R. Sutak).

https://doi.org/10.1016/j.csbj.2021.12.023
2001-0370/

mutualistic algal-bacterial interactions involving vitamin B12 [9,10] or iron [11].

Comparative studies of iron metabolism in different species are complicated by the virtual impossibility of achieving the same iron conditions in different cultures, particularly in time-course experiments, while the analysis of complex natural samples is biased by heterogeneity even in the dominant species. The aim of our study was to establish cocultivation experiments where each species in the community would be distinguishable by flow cytometry and present in quantities enabling homogenous detection of proteins, within a reasonable timeframe to observe the effect of nutritional changes. Such a system would provide equal iron conditions for each member of the consortia in time and allow us to study dynamic changes in the growth and proteomes of individual species.

2. Materials and methods

2.1. Cell culture

Amphidinium carterae (CCMP1314), *Bigelowiella natans* (CCMP2755), *Eutreptiella gymnastica* (K-0333), *Emiliania huxleyi* (CCMP371), *Heterocapsa triquetra* (CCMP449), *Phaeodactylum tricornutum* (CCMP2561), *Tetraselmis* sp. (CCMP961), *Thalassiosira oceanica* (CCMP1005) and *Thalassiosira pseudonana* (CCMP1335) were grown at 18 °C under a 12 h/12 h light (50 μmol m^{-2} s^{-1}) /dark regime in filtered modified f (Mf) medium, as described previously [12]. The composition of the Mf medium was as follows: 40 g/l sea salts; 75 mg/l $NaNO_3$; 2.66 mg/l NH_4NO_3; 22.8 mg/l $Na_2SiO_3{\cdot}5H_2O$; 15 mg/l NaH_2PO_4; 1 ml of trace metal stock (200 mg/l $MnCl_2{\cdot}4H_2O$; 40 mg/l $ZnSO_4{\cdot}7H_2O$; 20 mg/l $Na_2MoO_4{\cdot}2H_2O$; 14 mg/l $CoCl_2{\cdot}6H_2O$; 10 mg/l $Na_3VO_4{\cdot}nH_2O$; 10 mg/l $NiCl_2$; 10 mg/ml H_2SeO_3) and 1 ml of vitamin stock (20 mg/l thiamine-HCl, 1 mg/ml biotin, 1 mg/ml B12). The medium was buffered with 1 g/l HEPES (pH 7.5). Iron-rich conditions were achieved by the addition of 0.1 μM ferric citrate (1:20). To establish copper-deficient conditions, 10 μM BCS (bathocuproinedisulfonic acid disodium salt) was added to the growth medium. All chemicals, including growth medium reagents, were purchased from Sigma–Aldrich (USA).

2.2. Flow cytometry

Before each cocultivation experiment, starting cultures of *Amphidinium carterae*, *Bigelowiella natans, Eutreptiella gymnastica*, *Emiliania huxleyi*, *Heterocapsa triquetra*, *Phaeodactylum tricornutum*, *Tetraselmis* sp., *Thalassiosira oceanica* and *Thalassiosira pseudonana* were maintained under iron-rich (Mf medium with the addition of 0.1 μM ferric citrate) or iron-limited (Mf medium without iron addition) conditions for seven days. Cell counts for each species were determined on a Guava easyCyte 8HT flow cytometer (Luminex Corporation, USA). To study the effect of copper availability, *T. oceanica* and *T. pseudonana* cultures were additionally maintained under copper-deficient (Mf medium with the addition of 10 μM BCS) or copper-sufficient (without BCS addition) conditions. Starting cultures for the five consortia species (Fig. 1) contained 2.6×10^4 *A. carterae* and *Tetraselmis* sp. cells and 5.2×10^4*B. natans*, *E. huxleyi* and *T. oceanica* cells. Cultures were combined and grown for seven days under appropriate iron conditions in three biological replicates. On the seventh day, consortia were analyzed using a BD LSRFortessaTM SORP flow cytometer (BD Biosciences, USA) with a 488 nm laser (100 mW) for excitation and PerCP-Cy5.5 (BP710/50) and FITC (BP530/30) emission filters corresponding to red and green fluorescence parameters. Starting cultures for dual *Thalasiosira* cocultivation (Fig. 2) contained 7.5×10^4 *T. oceanica* and *T. pseudonana* cells. Cultures were combined, grown for seven days under appropriate iron and copper conditions in three biological replicates and analyzed using a Guava easyCyte 8HT flow cytometer with a 488 nm laser (150 mW) for excitation and Red-B (BP695/50) and Green-B (BP525/30) emission filters corresponding to red and green fluorescence parameters. Starting cultures in the consortia to study the effect of ferrioxamine B contained 5.2×10^4*B. natans* cells, 2.6×10^4 *A. carterae* cells and 2.6×10^4 cells of either *Tetraselmis* sp. or *E. gymnastica*. Cultures were combined, allowed to grow for seven days under iron-limited (without iron addition) or iron-rich (addition of 0.1 μM ferric citrate (1:20) or 0.1 μM ferrioxamine B (1:1.1)) conditions and measured using a Guava easyCyte 8HT flow cytometer with a 488 nm laser (150 mW) for excitation and Red-B (BP695/50) and Green-B (BP525/30) emission filters corresponding to red and green fluorescence parameters. All data were analyzed using FlowJo v10 software (BD Biosciences).

2.3. Proteomic analysis

Label-free whole-cell comparative proteomic analysis of *Amphidinium carterae*, *Bigelowiella natans*, *Heterocapsa triquetra* and *Phaeodactylum tricornutum* mixed cultures was performed in independent biological triplicates. Iron-rich (maintained in Mf medium with 0.1 μM ferric citrate) and iron-limited (Mf medium without iron addition) starting cultures containing 6×10^4 *A. carterae* cells, 1.25×10^5*B. natans* cells, 1.25×10^5*P. tricornutum* cells and 2×10^4*H. triquetra* cells were combined and allowed to grow for one day under appropriate iron conditions. At the beginning of the experiment, 0.1 μM ferric citrate was added to achieve iron enrichment in iron-limited cultures. At given timepoints (1, 6 and 24 h), cells were counted using flow cytometry and centrifuged (1000*g*; 5 min; 4 °C), and the dry pellet was subjected to proteomic analysis according to [13]. Detailed characteristics of the proteomic analysis are summarized in Table S2.

2.4. Statistical analysis

Single-OMIC analyses do not provide a deep understanding of biological systems. Thus, two-step normalization was employed to overcome hidden variation due to different cell numbers and variable expression levels. First, size-factor vector normalization was used, where the normalizing factor was estimated from cell counts using flow cytometry. Next, quantile normalization was used on cell count-normalized data, which is a technique for making two (or more) distributions identical in statistical properties. We used the *preprocessCore* package in R software [14]. This method uses the concept of a quantile–quantile plot in n-dimensions and is amenable for normalizations of multi-OMICS data. To detect the changes in variation due to two-step normalization, we used (s)PLS-DA: (sparse) partial least squares discriminant analysis in the R package *mixOmics* [15] and the area under the curve (AUC) for the extraction of sensitivity values, specificity of discriminations and corresponding p values.

2.5. Iron uptake

The incorporation of iron into protein complexes was analyzed by blue native PAGE as described in [16]. Prior to iron uptake experiments, cultures were grown in iron-deficient Mf medium (without added Fe) for 7 days. Then, 0.1 μM ^{55}Fe (29,600 MBq mg^{-1}) was added in the form of ferric citrate (1:20), ferric EDTA (1:10), ferrioxamine B (FOB; 1:1.1) or enterobactin (FeENT; 1:1.1) to the cell cultures and incubated for 24 h. Stock solutions of ^{55}Fe-labeled siderophores (FOB, FeENT) were prepared according to [4]. The cells were harvested by centrifugation and washed three times with ice-cold cultivation medium. Subsequently, the cells

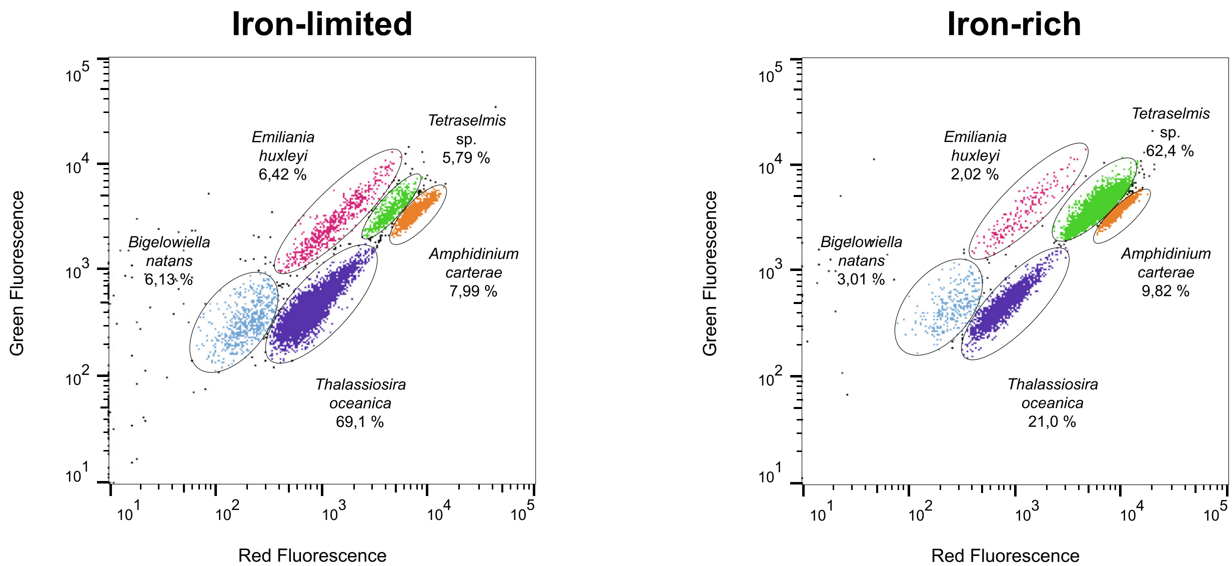

Iron-limited:

Subset Name	Forward Scatter	Green Fluorescence	Red Fluorescence	Count
A. carterae	54464	3345	7137	799
B. natans	23552	309	205	613
E. huxleyi	32320	2520	1211	642
Tetraselmis sp.	36800	3653	4521	579
T. oceanica	26496	413	767	6909
All Events	27648	462	808	10000

Iron-rich:

Subset Name	Forward Scatter	Green Fluorescence	Red Fluorescence	Count
A. carterae	57472	3507	9119	982
B. natans	20416	442	268	301
E. huxleyi	30464	3323	1122	642
Tetraselmis sp.	36416	3619	5674	579
T. oceanica	23616	466	772	6909
All Events	33280	3198	5059	10000

Fig. 1. Effect of iron availability on representative microalgal consortia. Flow cytograms of microalgal consortia containing five microalgal species (*B. natans*, *E. huxleyi*, *Tetraselmis* sp., *A. carterae* and *T. oceanica*) grown for one week under iron-limited or iron-rich conditions. Tables under flow cytograms contain median values for Forward Scatter, Green Fluorescence and Red Fluorescence parameters together with cell counts for each species. (For interpretation of the references to colour in this figure legend, the reader is referred to the web version of this article.)

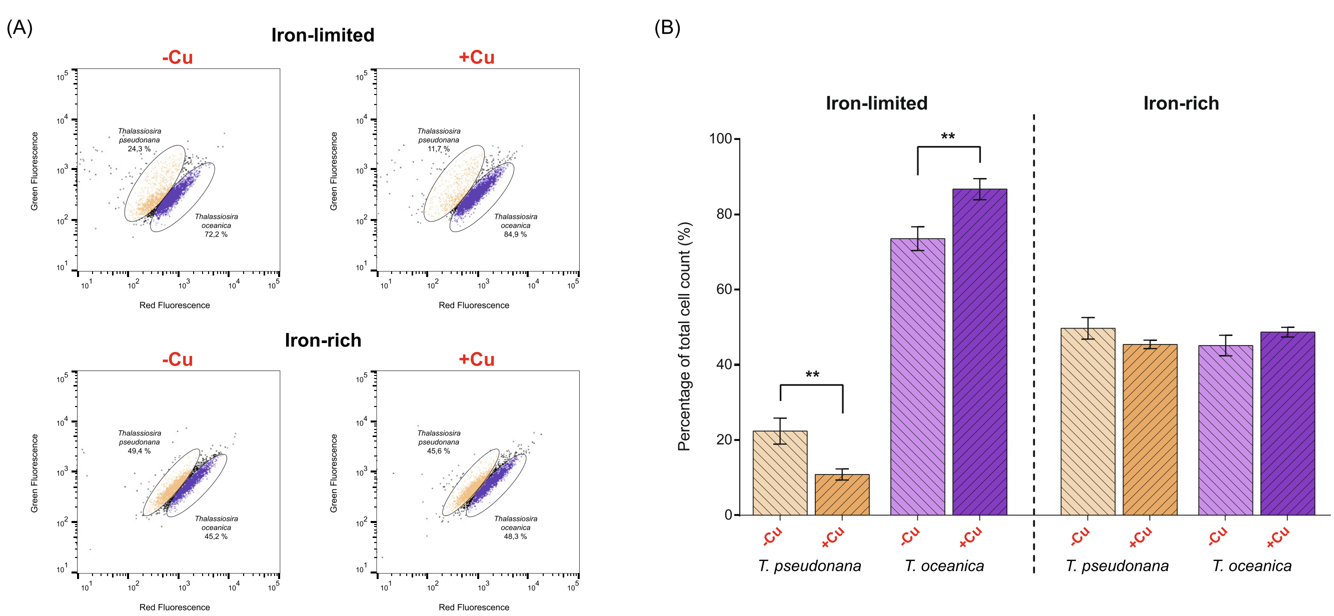

Fig. 2. Effect of iron and copper availability on coastal and oceanic *Thalassiosira*. (A) Flow cytograms with gates of two cocultivated species (*T. pseudonana* and *T. oceanica*) grown for one week under iron-limited or iron-rich conditions and copper-deprived (-Cu) or copper-sufficient (+Cu) conditions. (B) Percentage of total cell count for *T. oceanica* and *T. pseudonana* under iron-limited or iron-rich conditions and copper deprived (-Cu) or copper sufficient (+Cu) conditions, measured in three replicates (mean ± SD, ** p less than 0.01).

were disrupted by sonication in the presence of 1% digitonin, and protein complexes were separated by blue native PAGE using the Novex Native PAGE Bis–Tris Gel 4–16% system (Invitrogen) according to the manufacturer's protocol. The gels were vacuum-dried and autoradiographed for 5 days using a BAS-IP TR 2025 E tritium storage phosphor screen (GE Life Sciences) and visualized using a Typhoon FLA 7000 (GE Life Sciences).

2.6. Siderophore utilization

FOB coupled to a fluorescent moiety, nitrobenz-2-oxa-1,3-diazole (FOB-NBD), was previously synthesized as described by [17]. *A. carterae*, *B. natans*, *Tetraselmis* sp. and *E. gymnastica* were grown in iron-deficient Mf medium (without iron addition) in independent biological triplicates for seven days. FOB-NBD

(1 μM) was added to the cell cultures and incubated for 1, 3 and 6 h in the dark at 18 °C. Cultures were measured using a Guava easyCyte 8HT flow cytometer with a 488 nm laser (150 mW) for excitation and Yellow-B (BP583/26) emission filter to detect DFOB-NBD accumulated within cells. Data were analyzed using FlowJo v10 software.

3. Results

We were able to set up a series of experiments with different combinations of species distinguishable by flow cytometry, allowing us to study the effect of iron on the fitness of each member of the consortia. Species were chosen based on their ability to grow at the same temperature and light intensity at relatively similar rates, differences in iron requirements (low-iron-adapted *E. huxleyi* and *T. oceanica* vs. species with higher iron demand), distinguishability by flow cytometry and the availability of axenic strains. For all species, genomic and/or transcriptomic data are available, allowing interpretation of results at molecular level, particularly in proteomic analysis. The discriminability of chosen species in each experiment was ensured by setting the flow cytometric parameters for monoxenic cultures, in most cases red and green fluorescence corresponding to autofluorescence of their chlorophyll, phycoerythrin and carotenoid pigments. Importantly, the cell populations were analyzed under changing iron availability. As shown in Fig. S1, the cell population parameters changed significantly for *Amphidinium carterae*, *Eutreptiella gymnastica*, *Phaeodactylum tricornutum*, *Tetraselmis* sp., *Thalassiosira oceanica* and *Thalassiosira pseudonana*.

Fig. 1 illustrates a cocultivation system containing five species: the chlorarachniophyte *Bigelowiella natans*, the coccolithophore *Emiliania huxleyi*, the flagellated chlorophyte *Tetraselmis* sp., the dinoflagellate *Amphidinium carterae* and the diatom *Thalassiosira oceanica*. Species are clearly distinguishable under both iron-rich and iron-limiting conditions using red and green fluorescence, and as expected, low iron availability provided a competitive advantage for *E. huxleyi* and *T. oceanica*, species adapted to iron-limited ocean regions. Iron limitation resulted in a more than 3-fold increase in the community proportion of both microalgae after one week.

An exemplary experiment demonstrating adaptation to metal availability is depicted in Fig. 2. In this dual culture, two *Thalassiosira* species were cocultivated. While *T. oceanica* is an open-ocean, low-iron-adapted diatom employing copper-containing plastocyanin for electron transport from the cytochrome b_6f complex to PSI [18], *T. pseudonana* is a coastal strain with high iron demand and plastocyanin has been replaced by cytochrome c6 [19]. Consistent with these differences, cultivation under iron-limited conditions supported the growth of *T. oceanica,* while copper deprivation favored *T. pseudonana* when iron was limiting.

In an attempt to observe complex cellular responses to changing iron availability at the molecular level, we employed label-free comparative proteomics to analyze algal consortia of four selected species. Iron-limited cocultures were supplemented with iron (LR) and compared at different time points over a 24-hour time course with cells maintained under conditions of iron limitation (LL). After 24 h, proteomic profiles were also compared with cells maintained under conditions of long-term iron sufficiency (RR). Flow cytograms of the consortia at 24 h and 6 days after iron enrichment are depicted in Fig. S2. Proteins detected from all studied organisms are shown in Table S1. We detected 6100 unique proteins throughout all species and conditions: 3717 proteins from *A. carterae*, 972 proteins from *P. tricornutum*, 737 proteins from *H. triquetra* and 735 proteins from *B. natans*.

We used sparse partial least squares discriminant analysis (sPLS-DA) and the area under the curve (AUC) [15] to determine whether specific conditions of our experiment yielded significant changes in the proteomic profiles. Graphical results of sPLS discriminations (Fig. 3) demonstrate that the predictive performance for all comparisons was improved after cell count normalization. While long-term iron-rich cells (RR24 in Fig. 3) revealed perfect discrimination on all sPLS-DA panels regardless of the type of normalization (Comp. 2: AUC = 1, p = 0.006), iron-limited cells 24 h after enrichment (LR24 in Fig. 3) showed better predictive performances after cell count and quantile normalization (two-step normalization). The suitability of the two-step normalization is demonstrated in Fig. 3C, G, K, where iron-limited *A. carterae* cells were well separated 6 h after iron supplementation.

Upon iron enrichment, we were able to observe the downregulation of the homologs of proteins named the iron-starvation-induced proteins (or ISIPs) and upregulation of the light-harvesting complex subunits and fructose bisphosphate aldolase class II, in all analyzed species. For simplicity, we demonstrate an iron-induced response by analysis of preselected proteins whose abundance was expected to be affected by iron status (Table 1) in the proteomic data obtained for *P. tricornutum* and *A. carterae*, the two species with the best proteomic coverage. Within 1 h after iron enrichment, only 9 out of 102 preselected proteins detected in these two species had changed more than 2-fold (8 in *P. tricornutum* and 1 in *A. carterae*). Within 6 h after iron addition, the number of affected proteins increased to 23 (13 in *P. tricornutum* and 10 in *A. carterae*). After 24 h, 47 proteins had changed more than 2-fold (23 in *P. tricornutum* and 24 in *A. carterae*), similar to the difference observed between long-term iron-rich and iron-limited conditions. In general, the fastest induced proteins (which changed more than 2-fold within 6 h after iron enrichment) were the subunits of photosystem I (PSI): PsaC, PsaD, PsaE and PsaL; photosystem II (PSII): PsbV; cytochrome b6/f - PetA and ATP synthase - AtpE; the enzyme magnesium chelatase, which is involved in chlorophyll synthesis; and the iron-containing enzyme fructose bisphosphate aldolase class II (FBAII), which is replaced by metal-free FBAI [20]. Iron starvation-induced proteins and the *P. tricornutum* cellular repressor of E1A stimulated genes 1 (CREG1) were downregulated more than 2-fold 6 h after iron enrichment. These proteins are known to be major markers of iron limitation [12,21]. Proteins that changed more than 2-fold only 24 h after iron enrichment included other ISIPs, flavodoxins (downregulated) and ascorbate peroxidase, PsbC, SOD1 (upregulated). An interesting difference between *A. carterae* and *P. tricornutum* in the response to iron starvation was the regulation of light-harvesting complex subunits (LHCX). While one of the 3 detected LHC subunits (LHCX2) of *P. tricornutum* was upregulated under iron-limited conditions, which was also reported by [22], all 12 detected homologs of *A. carterae* LHCX were downregulated or unchanged, including the probable homolog of LHCX2 (CAMPEP_0176611302). LHCX2 is believed to be a regulator of nonphotochemical quenching (NPQ), the capacity of which is increased under iron-limited conditions [22]. The different responses of NPQ regulation to iron could reflect the different general light response flexibilities of both species. In their natural environment, bloom-forming dinoflagellates live in a stable stratified layer at the subsurface, usually below approximately 10 m depth, where illumination can sometimes be reduced to 1% [23]. As a result, *A. carterae* is genotypically adapted to low quantum flux densities and lacks an effective mechanism for de-excitation when excess light is absorbed [24]. On the other hand, planktonic diatoms, inhabiting turbulent surface waters, acclimatize to fluctuating light conditions better than dinoflagellates [23]. Diatoms are well known for their general light-response flexibility and potential for tuning their photosynthetic efficiency by NPQ under prolonged and potentially unfavorable conditions (reviewed in [25]).

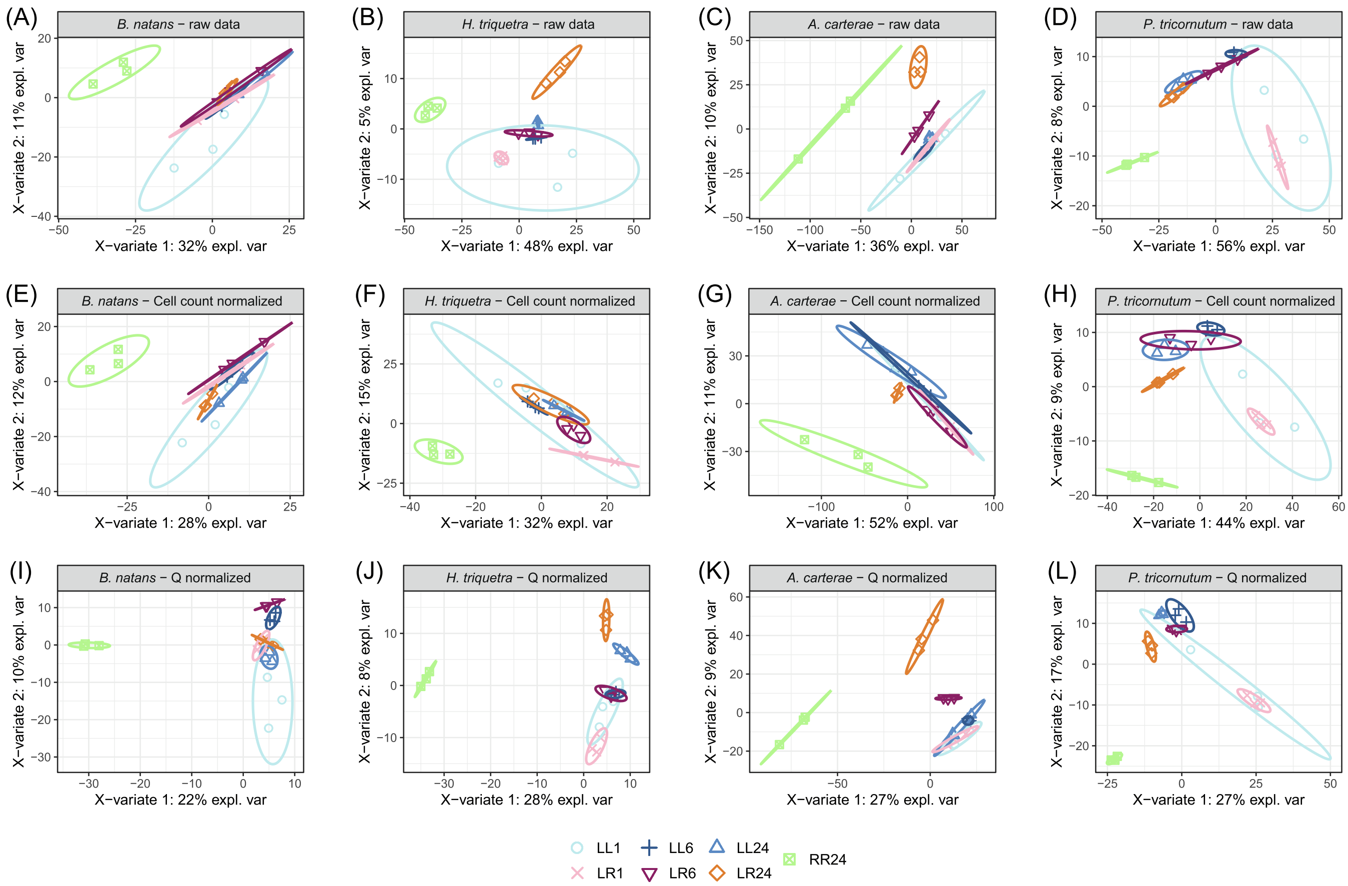

Fig. 3. Divergent patterns of protein abundances in raw and normalized datasets. Sparse PLS discriminant analysis revealed that raw data (A, B, C, D), cell count-normalized data (E, F, G, H) and quantile-normalized data after cell count normalization (I, J, K, L) had different predictive performances. We observed clear discriminations after cell count normalizations and even clearer discriminations after quantile normalizations, which further improved most of these discriminations (e.g., A, E, I). LL: long-term iron limitation, RR: long-term iron sufficiency, LR: iron enrichment. The number denotes time (hours) after beginning an experiment (after iron enrichment of LR cells).

Interestingly, while changes in the expression of the proteins most significantly affected by iron resupply were generally similar or more pronounced in cells maintained continuously under iron-rich conditions, the levels of ISIPs (and Creg1 in *P. tricornutum*) were lower in resupplied cells than in those cultivated under conditions of long-term iron sufficiency. We believe that cells grown under long-term iron-sufficient conditions maintain a stable level of basal expression of these strong iron stress markers, while it is possible that sudden iron enrichment led to their overrepression. This can be explained by the continuous utilization of iron sparing pathways in long-term iron-deprived cells.

An important observation was made when the siderophore ferrioxamine B (FOB) was used as an iron source in cultures containing *B. natans* and *A. carterae* with *Tetraselmis* sp. (Fig. 4A), or the euglenid *E. gymnastica* (Fig. 4B). In contrast to other members of the consortia, the growth of *A. carterae* was stimulated by the addition of iron in the form of FOB. This observation indicates the presence of machinery responsible for siderophore acquisition. We thus decided to investigate the ability to acquire iron from siderophores in *A. carterae* as well as in other species whose growth in these cocultures was suppressed when iron was supplied as FOB. We exposed *A. carterae*, *B. natans*, *Tetraselmis* sp. and *E. gymnastica* monocultures to ^{55}Fe chelated by citrate (a relatively weak iron chelator), EDTA (a strong chelator) or two siderophores (hydroxamate-type FOB and catecholate-type enterobactin). The incorporation of iron from those sources into cellular proteins was visualized after separation on blue native electrophoresis gels. The results are presented in Figs. 5A and S3, where it is evident that only *A. carterae* was able to effectively utilize iron from FOB, consistent with our flow cytometry results. None of the species tested in our study showed efficient incorporation of iron into cellular proteins when iron was chelated by enterobactin, including *A. carterae,* indicating that this dinoflagellate preferably acquires hydroxamate-type siderophores. Experiments with the fluorescent conjugate of desferrioxamine B complexed with iron (FOB-NBD) further demonstrated the capacity for siderophore iron utilization by *Amphidinium*. The fluorescence of this siderophore conjugate is quenched by iron; therefore, the release of iron from siderophores can be monitored by flow cytometry. Fig. 5B, C presents an effective acquisition of iron from FOB by *A. carterae* traced in time, which contrasts with the absence of iron release from the siderophore by the rest of the members of the algal consortia (Fig. S4). These observations are additionally supported by our complex proteomic analysis, where we identified among *A. carterae* proteins downregulated by iron resupply, a potential siderophore binding protein that showed a 2.5-fold decrease 24 h after iron enrichment (CAMPEP_0176544322, Table S1). It is a homolog of the *P. tricornutum* FBP1 protein that was recently shown to participate in iron acquisition from hydroxamate siderophores [26]. Homologs of FBP1 protein, identified in different marine microalgae, were shown to share a common ancestor with hydroxamate siderophore lipoprotein receptors found in gram-positive bacteria. The protein from *A. carterae* appears to be among the closely related homologs to the actinobacterial iron siderophore ABC transporter solute binding proteins [26].

Table 1
Effect of iron availability on the abundance of selected *A. carterae* and *P. tricornutum* proteins. Data represent fold change in protein abundance in iron-limited (LL) cells 24 h after iron supply (LR) and differences between iron-limited cells and cells grown under long-term iron-rich conditions (RR). *A. carterae* (highlighted in green) and *P. tricornutum* (highlighted in red) cells were cocultivated in a consortium that included *B. natans* and *H. triquetra*. An asterisk (*) in the protein name denotes fold change higher than 2-fold as early as 6 h after iron enrichment.

Protein name	Organism	Protein ID	24 h LL-LR	24 h LL-RR
Ascorbate peroxidase*	Ac	CAMPEP_0176532796	4,6	4,0
Ascorbate peroxidase*	Pt	tr|B7S491|B7S491_PHATC	1,1	6,5
AtpE*	Ac	CAMPEP_0176614664	1,7	5,2
AtpE	Pt	sp|A0T0D1|ATPE_PHATC	1,3	1,7
AtpG	Ac	CAMPEP_0176550046	1,6	1,1
AtpG	Ac	CAMPEP_0176641968	1,8	1,4
AtpG	Pt	sp|A0T0E8|ATPF2_PHATC	1,8	1,1
CREG1	Ac	CAMPEP_0176541126	−2,1	−4,3
CREG1*	Pt	tr|B7G9B3|B7G9B3_PHATC	−23,5	−2,0
Fba classI	Ac	CAMPEP_0176532332	1,2	−1,1
Fba classI	Ac	CAMPEP_0176622298	−1,2	−2,0
Fba classI	Pt	tr|B7GE67|B7GE67_PHATC	−5,3	−4,3
Fba classII	Ac	CAMPEP_0176610888	1,9	2,8
Fba classII	Ac	CAMPEP_0176614222	−1,2	−1,1
Fba classII	Ac	CAMPEP_0176531794	−1,3	−1,1
Fba classII*	Ac	CAMPEP_0176638318	1,4	1,5
Fba classII	Pt	tr|B7G4R3|B7G4R3_PHATC	−1,7	1,0
Fba classII*	Pt	tr|B7S3N8|B7S3N8_PHATC	4,6	4,4
Fba classII	Pt	tr|B7G9G9|B7G9G9_PHATC	1,4	4,3
Flavodoxin	Ac	CAMPEP_0176557388	−1,5	−4,3
Flavodoxin	Ac	CAMPEP_0176611622	−1,5	−3,9
Flavodoxin	Pt	tr|B7GCM3|B7GCM3_PHATC	−6,3	−2,9
Gsr_2	Ac	CAMPEP_0176670554	1,4	1,3
Gsr_2	Ac	CAMPEP_0176627754	−1,1	−1,6
Gsr_2	Ac	CAMPEP_0176625460	1,0	−2,3
Gsr_2	Ac	CAMPEP_0176635824	−1,2	−1,4
Gsr_2	Ac	CAMPEP_0176642616	1,1	−1,8
Gsr_2	Pt	tr|B7G326|B7G326_PHATC	−1,7	−1,2
Gsr_2	Pt	tr|B7G9G3|B7G9G3_PHATC	1,1	1,2
Gsr_2	Pt	tr|B7FZC3|B7FZC3_PHATC	NA	1,3
Gsr_2	Pt	tr|B7G9Q1|B7G9Q1_PHATC	−2,1	1,5
Gsr_2	Pt	tr|B7FVM3|B7FVM3_PHATC	−1,3	−1,1
ISIP2*	Ac	CAMPEP_0176513402	−4,6	−1,7
ISIP2*	Ac	CAMPEP_0176599704	−5,2	−2,8
ISIP2*	Ac	CAMPEP_0176611892	−7,8	−1,4
ISIP2	Pt	tr|B7FYL4|B7FYL4_PHATC	−1,6	−2,2
ISIP2a	Pt	tr|B7FYL2|B7FYL2_PHATC	−6,4	−2,4
ISIP2b*	Pt	tr|B7G9B1|B7G9B1_PHATC	−13,8	−4,5
ISIP3	Ac	CAMPEP_0176533694	−4,1	−2,6
ISIP3*	Pt	tr|B7G4H8|B7G4H8_PHATC	−6,5	−4,8
RbcL	Ac	CAMPEP_0176611690	1,3	1,8
RbcL	Pt	sp|Q9TK52|RBL_PHATC	−1,1	1,3
Lhcx	Ac	CAMPEP_0176610792	3,0	2,4
Lhcx	Ac	CAMPEP_0176557516	1,1	1,9
Lhcx	Ac	CAMPEP_0176610966	2,2	4,0
Lhcx	Ac	CAMPEP_0176638146	2,2	1,6
Lhcx	Ac	CAMPEP_0176532122	1,5	1,3
Lhcx	Ac	CAMPEP_0176621150	1,5	2,0
Lhcx	Ac	CAMPEP_0176532000	1,4	1,6
Lhcx	Ac	CAMPEP_0176610776	2,4	2,4
Lhcx	Ac	CAMPEP_0176536776	1,4	1,3
Lhcx	Ac	CAMPEP_0176638270	1,5	1,1
Lhcx	Ac	CAMPEP_0176611302	1,7	1,8
Lhcx	Ac	CAMPEP_0176638538	1,5	1,7
Lhcx	Pt	tr|B7FYL0|B7FYL0_PHATC	−1,1	1,3
Lhcx*	Pt	tr|B7FVF9|B7FVF9_PHATC	−1,6	1,8
Lhcx2	Pt	tr|B7FR60|B7FR60_PHATC	−5,5	−4,7
Magnesium chelatase*	Ac	CAMPEP_0176575976	2,3	3,1
Magnesium chelatase	Pt	tr|A0T0B5|A0T0B5_PHATC	1,8	1,3
Magnesium chelatase	Pt	tr|B7FTA2|B7FTA2_PHATC	1,5	2,8
Magnesium chelatase*	Pt	tr|B5Y3F4|B5Y3F4_PHATC	3,1	1,8
PetA	Ac	CAMPEP_0176611648	1,6	1,8
PetA*	Ac	CAMPEP_0176535836	5,5	6,1
PetA	Pt	sp|A0T0C9|CYF_PHATC	2,4	2,9
PetB	Ac	CAMPEP_0176617416	1,5	−1,2
PetB	Pt	sp|A0T0B8|CYB6_PHATC	3,1	3,6
PsaA	Ac	CAMPEP_0176651446	1,8	−1,5
PsaA	Pt	sp|A0T0M7|PSAB_PHATC	2,9	5,1
PsaD	Ac	CAMPEP_0176533106	2,9	2,1
PsaD	Ac	CAMPEP_0176564748	2,0	1,8
PsaD*	Ac	CAMPEP_0176538974	8,8	9,3

Table 1 (*continued*)

Protein name	Organism	Protein ID	24 h LL-LR	24 h LL-RR
PsaD	Pt	tr|A0T0B9|A0T0B9_PHATC	4,4	3,5
PsaL	Ac	CAMPEP_0176639782	2,5	1,3
PsaL	Ac	CAMPEP_0176557554	2,3	1,5
PsaL*	Ac	CAMPEP_0176553508	2,9	−1,1
PsaL*	Ac	CAMPEP_0176533490	2,3	1,6
PsaL*	Pt	sp|A0T0M6|PSAL_PHATC	2,4	3,9
PsbC	Ac	CAMPEP_0176554406	2,1	1,5
PsbC	Pt	tr|A0T096|A0T096_PHATC	2,6	3,5
PsbV*	Ac	CAMPEP_0176612574	2,9	3,9
PsbV*	Pt	sp|A0T0C6|CY550_PHATC	3,3	5,1
SOD1	Ac	CAMPEP_0176541592	1,0	1,3
SOD1	Ac	CAMPEP_0176525294	1,2	1,9
SOD1	Pt	tr|B7G0L6|B7G0L6_PHATC	1,0	1,9

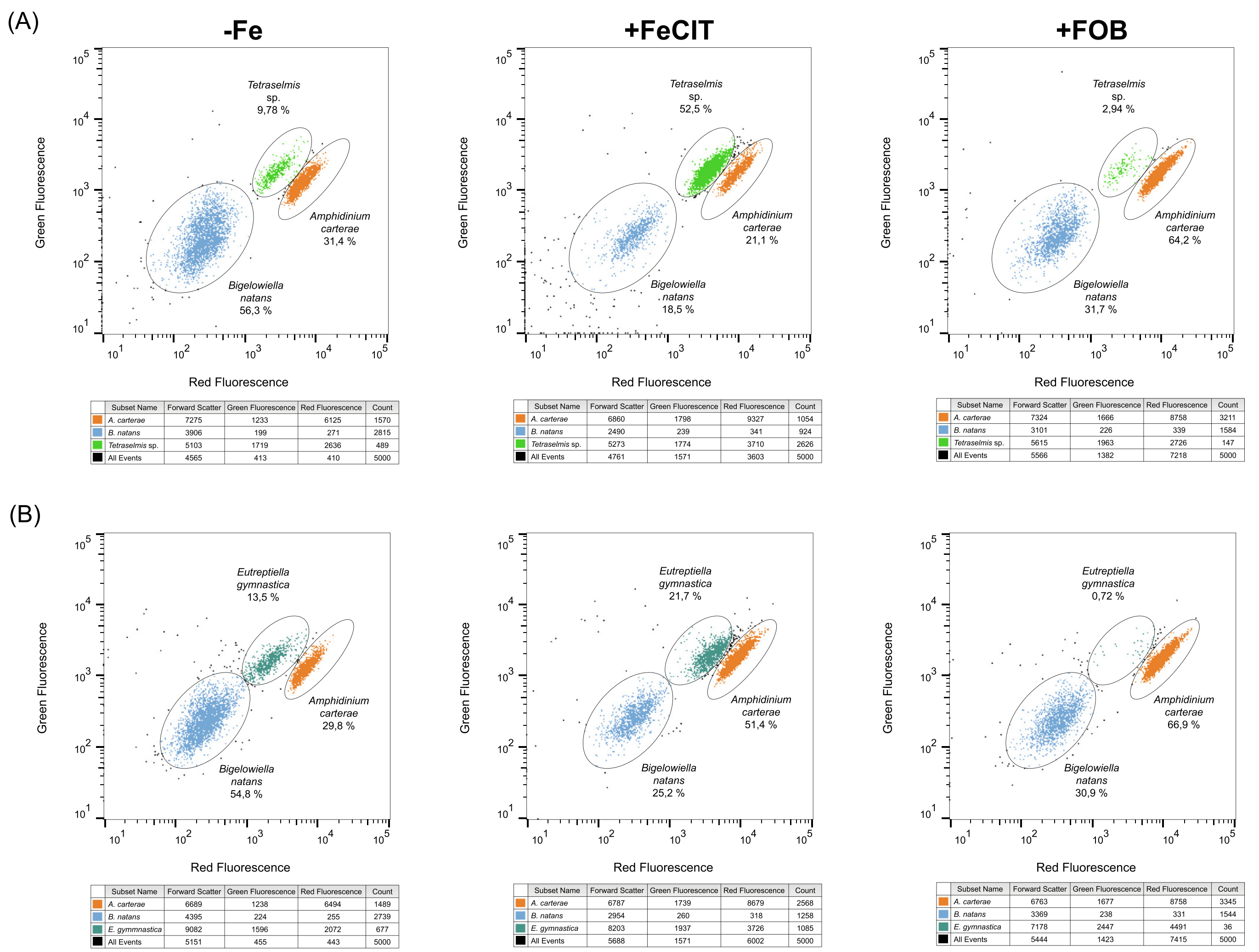

Fig. 4. Effect of FOB siderophore on cocultivated microalgae. Flow cytograms of two microalgal consortia, each containing three algal species ((A) *B. natans*, *Tetraselmis* sp., *A. carterae*; (B) *B. natans*, *E. gymnastica*, *A. carterae*) grown under iron-limited condition (-Fe), with iron supplemented in the form of ferric citrate (+FeCIT) and with iron provided as ferrioxamine B (+FOB). Tables under flow cytograms contain median values for Forward Scatter, Green Fluorescence and Red Fluorescence parameters together with cell counts for each species. (For interpretation of the references to colour in this figure legend, the reader is referred to the web version of this article.)

4. Discussion

Determining the effect of changing iron conditions on phytoplankton is important and challenging. In our study, we established a cocultivation system with different combinations of species that allowed us to follow the effects of iron availability on members of the consortia by simple enumeration based on differences in fluorescence properties. Choosing species that have,

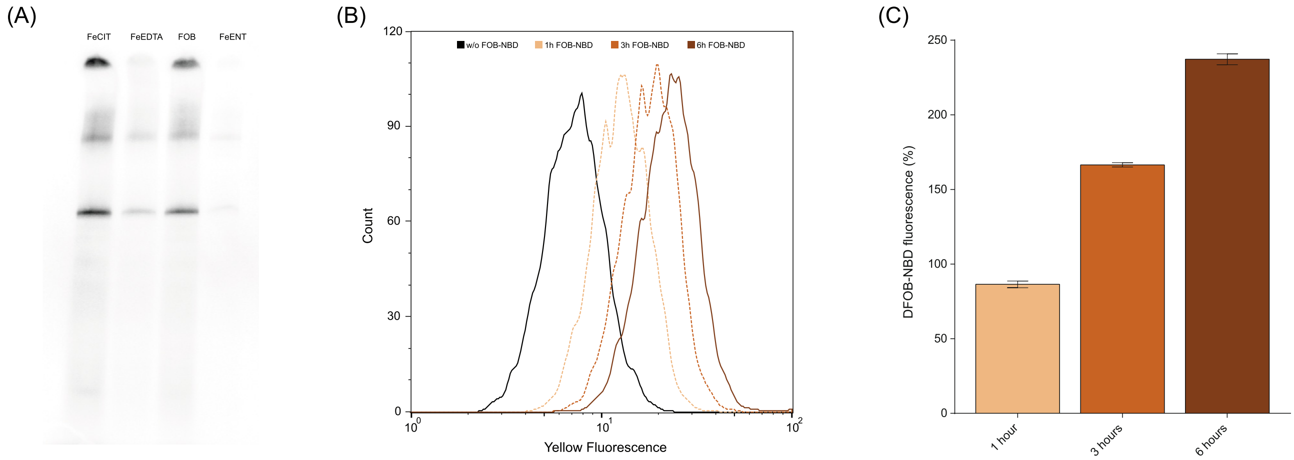

Fig. 5. Utilization of iron from FOB siderophore by *A. carterae.* (A) Incorporation of ^{55}Fe into *A. carterae* protein complexes determined by blue native electrophoresis separation of total cell extracts. Iron was supplemented in four different forms: FeCIT – ferric citrate (1:20), FeEDTA – ferric EDTA (1:10), FOB – ferrioxamine B (1:1.1), and FeENT – enterobactin (1:1.1). (B, C) *A. carterae* cells grown in iron-deficient medium for 7 days were supplemented with 1 μM of the fluorescent conjugate of desferrioxamine B complexed with iron (FOB-NBD) and incubated for 1, 3 and 6 h. Intracellular accumulation of a nonquenched siderophore analog (after removal of iron) was measured on a flow cytometer using a yellow fluorescence detector (583/26 nm) and blue excitation laser (488 nm). (B) Representative histogram. (C) Fluorescence of DFOB-NBD (mean ± SD, n = 3). (For interpretation of the references to colour in this figure legend, the reader is referred to the web version of this article.)

at least to some degree, available genomes/transcriptomes, enabled us to study the molecular mechanisms behind adaptation to iron limitation via a proteomic analysis of complex samples. We were able to detect significant iron-induced changes in algal proteomes, including well-known markers of iron limitation, such as ISIPs, FBA, LHCX and subunits of PSI, ATP synthase and Cytochrome b6/f [20,22,27,28]. Time course analysis revealed a dynamic response to iron enrichment evidenced by a number of proteins that significantly changed as early as 6 h after iron supplementation. Changes in proteomes between iron-rich and iron-limited cells appear to be reached within 24 h after iron supply to iron-limited species.

Our study provides a proof-of-concept that it is possible, when suitable species and conditions are chosen, to reveal proteins whose expression is most significantly affected by nutrients in complex algal cultures, thus representing candidate markers for nutrient (and other) stress in natural marine phytoplankton. Such an experimental design represents an alternative to cocultivation systems where species are separated by membranes permeable to nutrients and metabolites but not cells. This system was successfully employed, for example, to describe the impact of *K. brevis* allelopathy on competing phytoplankton [29]. The advantage of our experimental design lies in the fact that it allows physiological and molecular analyses of phytoplankton consortia while allowing physical contact between the species. This design can be employed in studies involving processes within the phycosphere, such as bacterial-algal mutualism.

Importantly, our study showed that it is possible to analyze, with reasonable efficiency, proteomic changes in mixed cultures for species without well-annotated genomes, with analysis employing available transcriptomes. It is axiomatic that proteomic analyses of a multispecies model system have limitations, which were observable in the case of *B. natans* and *H. triquetra* in our study. Fewer than 750 proteins were detected for each of the two species. However, proteome coverage can be expanded by increasing the mass spectrometry detection capacity, e.g., by employing peptide or predigestion protein fractionation prior to proteomic analysis. Alternatively, FACS may be used for the separation of microalgal populations to allow maximal proteome coverage for each species in the consortium.

We touched an important methodological question of how to normalize proteomic data from complex ecological mixtures. The combination of sPLS discriminant analysis and the extraction of p values from AUC analysis helped us to identify the effect of two types of consecutive normalizations. The raw data in Fig. 3A, B, C, D show high variances and group overlaps due to noise coming from different cell numbers per species. When we applied size-factor vector normalization from the cell counts, the variances slightly decreased, but some overlaps were still visible (Fig. 3E, F, G, H). To decrease the influence of outliers and differences in the abundances within proteomes, we used quantile normalization (second step) on cell count-normalized data. The effect of two-step normalization is obvious in Fig. 3I, J, K, L where the ellipses over the group data are smaller and overlap less with other groups. The important message here is that the predictive performance of proteomic analyses strongly depends on the type of data normalization, and that both the initial variance and the influence of outliers may well be sustained when using the two-step normalization presented in this manuscript.

Little is known about iron acquisition in *Amphidinium carterae*, although this model dinoflagellate was used more than 40 years ago to suggest the significance of grazing on phytoplankton in iron recycling in marine environment [30]. The main finding that emerged from our study was the ability of *A. carterae* to utilize iron from FOB siderophores. Reports about the use of siderophore-bound iron by eukaryotic phytoplankton are rare [11,31,32], and molecules involved in this iron uptake pathway are only suggested for the model diatom *P. tricornutum* [4,26]. It is now believed that siderophores represent an important part of ocean microbial iron cycling, showing changing abundance and composition across ocean regions with varying iron availability [33]. The ability to utilize iron from xenosiderophores may give *A. carterae* an advantage in ecosystems where such form of iron is abundant. In fact, cocultivation with bacteria has been shown to promote the growth of *A. carterae* in nutrient-limited media, including conditions of trace-metal limitation [34]. Importantly, our proteomic analysis revealed that the *A. carterae* homolog of siderophore binding protein was dynamically regulated by iron availability. The fact that this protein has been shown to be involved in siderophore acquisition in the taxonomically distant diatom *P. tricornutum* highlights the effect of a nutritionally poor ocean environment on molecular evolution. This fascinating phenomenon is particularly obvious through the virtually universal presence of phytotransferrins in marine eukaryotic phytoplankton. Notably, the iron enrichment-induced downregulation of these recently discovered major players in iron uptake was also detected in all species of our coculture model. Both phytotransferrin-mediated and siderophore-bound iron uptake mechanisms are most likely based on elaborate machinery involving endocytosis [35]; thus, this adaptation to life under iron-limited conditions requires complex fine-tuning.

Our study demonstrates an efficient tool that allowed us to follow community dynamics in mixed cultures of model eukaryotic phytoplankton species and determine concomitant changes at the molecular level. We believe that such an approach, complimentary to field investigation, may be employed to better understand phytoplankton responses to environmentally relevant changes in nutrient availability, pH or temperature.

CRediT authorship contribution statement

Ronald Malych: Data curation, Investigation, Visualization, Writing – original draft. **Pavel Stopka:** Formal analysis, Methodology, Writing – review & editing. **Jan Mach:** Methodology, Validation, Writing – review & editing. **Eva Kotabová:** Investigation, Methodology. **Ondřej Prášil:** Validation, Writing – review & editing. **Robert Sutak:** Conceptualization, Funding acquisition, Project administration, Supervision, Validation, Writing – original draft.

Declaration of Competing Interest

The authors declare that they have no known competing financial interests or personal relationships that could have appeared to influence the work reported in this paper.

Acknowledgements

The project was supported by the Czech Science Foundation (18-07822S), CZ.02.1.01/0.0/0.0/16_019/0000759 CePaViP provided by The European Regional Development Fund and Ministry of Education, Youth and Sports of the Czech Republic (MEYS), MiCoBion project funded from EU Horizon 2020 (No 810224). Acknowledgment to Karel Harant and Pavel Talacko from Laboratory of Mass Spectrometry, Biocev, Charles University, Faculty of science, where proteomic and mass spectrometric analysis had been done. We acknowledge the Imaging Methods Core Facility at BIOCEV for their support with obtaining flow cytometry data presented in this paper.

In a memory of Emmanuel Lesuisse.

Appendix A. Supplementary data

Supplementary data to this article can be found online at https://doi.org/10.1016/j.csbj.2021.12.023.

References

[1] Martin JH, Gordon RM, Fitzwater SE. Iron Limitation. Limnol Oceanogr 1991;36:1793–802.
[2] Sunda WG, Huntsman SA. Iron uptake and growth limitation in oceanic and coastal phytoplankton. Mar Chem 1995;50(1-4):189–206.
[3] Lis H, Shaked Y, Kranzler C, Keren N, Morel FMM. Iron bioavailability to phytoplankton: an empirical approach. ISME J 2015;9(4):1003–13.
[4] Kazamia E, Sutak R, Paz-Yepes J, Dorrell RG, Vieira FRJ, Mach J, et al. Endocytosis-mediated siderophore uptake as a strategy for Fe acquisition in diatoms. Sci Adv 2018;4(5). https://doi.org/10.1126/sciadv.aar4536.
[5] Lampe RH, Mann EL, Cohen NR, Till CP, Thamatrakoln K, Brzezinski MA, et al. Different iron storage strategies among bloom-forming diatoms. Proc Natl Acad Sci U S A 2018;115(52):E12275–84.
[6] Hutchins DA, Boyd PW. Marine phytoplankton and the changing ocean iron cycle. Nat Clim Chang 2016;6(12):1072–9.
[7] Du ZY, Zienkiewicz K, Vande PN, et al. Algal-fungal symbiosis leads to photosynthetic mycelium. Elife 2019;8:1–22.
[8] Fisher BS, Estraño CE, Cole JA, Talamas-Rohana P. Modeling long-term host cell-Giardia lamblia interactions in an in vitro co-culture system. PLoS ONE 2013;8(12):e81104. https://doi.org/10.1371/journal.pone.0081104.
[9] Haines KC, Guillard RRL. Growth of vitamin B12-requiring marine diatoms in mixed laboratory cultures with vitamin b12-producing marine bacteria. J Phycol 1974;10:245–52.
[10] Croft MT, Lawrence AD, Raux-Deery E, Warren MJ, Smith AG. Algae acquire vitamin B12 through a symbiotic relationship with bacteria. Nature 2005;438 (7064):90–3.
[11] Amin SA, Green DH, Hart MC, et al. Photolysis of ion – siderophore chelates promotes bacteria – algal mutualism Photolysis of iron – siderophore chelates promotes bacterial – algal mutualism. Environ Sci 2017;106:2–7.
[12] Kotabova E, Malych R, Pierella Karlusich JJ, Kazamia E, Eichner M, Mach J, et al. Complex response of the chlorarachniophyte bigelowiella natans to iron availability. mSystems 2021;6(1). https://doi.org/10.1128/mSystems.00738-20.
[13] Mach J, Bíla J, Ženíšková K, Arbon D, Malych R, Glavanakovová M, et al. Iron economy in Naegleria gruberi reflects its metabolic flexibility. Int J Parasitol 2018;48(9-10):719–27.
[14] Bolstad BM, Irizarry RA, Astrand M, Speed TP. A comparison of normalization methods for high density oligonucleotide array data based on variance and bias. Bioinformatics 2003;19(2):185–93.
[15] Lê Cao KA, Boitard S, Besse P. Sparse PLS discriminant analysis: Biologically relevant feature selection and graphical displays for multiclass problems. *BMC Bioinformatics* 2011;**12**, DOI: 10.1186/1471-2105-12-253.
[16] Scheiber IF, Pilátová J, Malych R *et al.* Copper and iron metabolism in: Ostreococcus tauri -the role of phytotransferrin, plastocyanin and a chloroplast copper-transporting ATPase. *Metallomics* 2019;**11**:1657–66.
[17] Ouchetto H, Dias M, Mornet R, Lesuisse E, Camadro J-M. A new route to trihydroxamate-containing artificial siderophores and synthesis of a new fluorescent probe. Bioorganic Med Chem 2005;13(5):1799–803.
[18] Peers G, Price NM. Copper-containing plastocyanin used for electron transport by an oceanic diatom. Nature 2006;441(7091):341–4.
[19] Blaby-Haas CE, Merchant SS. Regulating cellular trace metal economy in algae. Curr Opin Plant Biol 2017;39:88–96.
[20] Caputi L, Carradec Q, Eveillard D, Kirilovsky A, Pelletier E, Pierella Karlusich JJ, et al. Community-level responses to iron availability in open ocean plankton ecosystems. Global Biogeochem Cycles 2019;33(3):391–419.
[21] Marchetti A, Schruth DM, Durkin CA, Parker MS, Kodner RB, Berthiaume CT, et al. Comparative metatranscriptomics identifies molecular bases for the physiological responses of phytoplankton to varying iron availability. Proc Natl Acad Sci USA 2012;109(6):E317–25. https://doi.org/10.1073/pnas.1118408109.
[22] Taddei L, Stella GR, Rogato A, Bailleul B, Fortunato AE, Annunziata R, et al. Multisignal control of expression of the LHCX protein family in the marine diatom Phaeodactylum tricornutum. J Exp Bot 2016;67(13):3939–51.
[23] Zhou L, Wu S, Gu W, et al. Photosynthesis acclimation under severely fluctuating light conditions allows faster growth of diatoms compared with dinoflagellates. BMC Plant Biol 2021;21:1–14.
[24] Samuelsson G, Richardson K. Photoinhibition at low quantum flux densities in a marine dinoflagellate (Amphidinium carterae). Mar Biol 1982;70(1):21–6.
[25] Lacour T, Babin M, Lavaud J, Kroth P. Diversity in xanthophyll cycle pigments content and related nonphotochemical quenching (NPQ) among microalgae: implications for growth strategy and ecology. J Phycol 2020;56(2):245–63.
[26] Coale TH, Moosburner M, Horák A, Oborník M, Barbeau KA, Allen AE. Reduction-dependent siderophore assimilation in a model pennate diatom. Proc Natl Acad Sci U S A 2019;116(47):23609–17.
[27] Behnke J, LaRoche J. Iron uptake proteins in algae and the role of Iron Starvation-Induced Proteins (ISIPs). Eur J Phycol 2020;55(3):339–60.
[28] Allen AE, LaRoche J, Maheswari U, Lommer M, Schauer N, Lopez PJ, et al. Whole-cell response of the pennate diatom Phaeodactylum tricornutum to iron starvation. Proc Natl Acad Sci U S A 2008;105(30):10438–43.
[29] Poulson-Ellestad KL, Jones CM, Roy J, Viant MR, Fernandez FM, Kubanek J, et al. Metabolomics and proteomics reveal impacts of chemically mediated competition on marine plankton. Proc Natl Acad Sci U S A 2014;111 (24):9009–14.
[30] Frey BE, Small LF. Recycling of metabolized iron by the marine dinoflagellate amphidinium carterae. J Phycol 1979;15:405–9.
[31] Maldonado MT, Price NM. Reduction and transport of organically bound iron by Thalassiosira oceanica (Bacillariophyceae). J Phycol 2001;37(2):298–310.
[32] Strzepek RF, Maldonado MT, Hunter KA, Frew RD, Boyd PW. Adaptive strategies by Southern Ocean phytoplankton to lessen iron limitation: uptake of organically complexed iron and reduced cellular iron requirements. Limnol Oceanogr 2011;56(6):1983–2002.
[33] Boiteau RM, Mende DR, Hawco NJ, McIlvin MR, Fitzsimmons JN, Saito MA, et al. Siderophore-based microbial adaptations to iron scarcity across the eastern Pacific Ocean. Proc Natl Acad Sci U S A 2016;113(50):14237–42.
[34] Park BS, Erdner DL, Bacosa HP, Liu Z, Buskey EJ. Potential effects of bacterial communities on the formation of blooms of the harmful dinoflagellate Prorocentrum after the 2014 Texas City "Y" oil spill (USA). Harmful Algae 2020;95:101802. https://doi.org/10.1016/j.hal.2020.101802.
[35] Sutak R, Camadro JM, Lesuisse E. Iron Uptake Mechanisms in Marine Phytoplankton. Front Microbiol 2020;11:1–14.